THE EGF ROUND ROBIN ON NUMERICAL EPFM

L.H. LARSSON*

This paper discusses the results of a round robin on numerical analysis in elastic-plastic fracture mechanics performed in the framework of the European Group on Fracture. The chosen problem was a CT-specimen for which experimental results were available from another EGF round robin. Only the specimen geometry and the material tensile curve were given, all the options of the analysis were free.

A total of 43 solutions in plane strain, plane stress and 3D were delivered by 22 participants. Comparisons of the solutions between themselves and with the experimental results are made and the reasons for the scatter are discussed.

INTRODUCTION

After a first numerical round robin on EPFM (see Larsson (1)) performed in 1980 there was a strong interest inside the European Group on Fracture (EGF) to pursue such activities. It was considered that round robins are a good means to get a picture of what kind of accuracy can be expected from non-linear analysis of cracked bodies that an increasing number of organisations is applying for safety assessments. This community applies a wide variety of computer codes and numerical methods. The first round robin showed that correspondingly, there is a large scatter of the results which reflects in some way the reliability of such analysis. One does not get much comfort from the statement that a few advanced laboratories possess the good techniques and the necessary know-how if in other places widely diverging results are likely to be obtained. The transfer of know-how and the thrust towards the elaboration of recommendations for the correct performance of EPFM numerical analysis are obviously amongst the major fall-outs of round robins.

The working party on numerical analysis of the EPFM task group of the EGF started the second round robin in 1982. The main problem, treated in the so-called Phase 2, was performed from June 1982 to the end of 1983 and regarded a CT-specimen. This time the chosen problem was intended to get not only code-to-code comparisons but also a confrontation with experimental results which became available afterwards.

A general presentation of this round robin was given by Larsson (2). The present paper starts with a short description of the definition of the round robin, the classification of the numerical solutions and data processing. After a comparison of the characteristics of the various types of

* Commission of the European Communities, Joint Research Centre, Ispra Establishment, 21020 Ispra, Italy

solutions, the bulk of the paper is devoted to a discussion of the most suitable methods of numerical analysis for EPFM problems. This part of the paper is based on the results of a meeting of the participants held after the closure of Phase 2. Even if consensus was not reached on all points, at least some preferred options emerged. On the other hand, the next phase of the round robin was defined in such a way as to throw light on several problems remained unresolved.

Table 1 shows the list of the 22 participating organizations with the names of the correspondents. They represent 9 European countries and one international organization.

TABLE 1 - Participants

M.A.Astiz	Madrid Technical University	Spain
A.Bakker	Delft University of Technology	The Netherlands
S.Bhandari	Novatome	France
B.A.Bilby	The University of Sheffield	U.K.
M.H.Bleackley and C.E.Turner	Imperial College, London	U.K.
J.Carlsson	Royal Institute of Technology	Sweden
J.L.Cheissoux	CEA, Cadarache	France
J.Van de Eickhoff	TNO, Delft	The Netherlands
H.J.Golembiewski	KWU, Erlangen	Germany
L.Grueter	Interatom	Germany
O.Gunneskov	RISØ National Laboratory	Denmark
T.K.Hellen and W.S.Blackburn	CEGB	U.K.
K.Ikonen	Technical Research Centre	Finland
A.P.Kfouri	The University of Sheffield	U.K.
L.Lamain	JRC, Ispra	CEC
D.Munz	University Karlsruhe	Germany
J.Olschewski	BAM, Berlin	Germany
J.Prij	ECN, Petten	The Netherlands
W.Schmitt	Fraunhofer-Institut, IWM Freiburg	Germany
I.J.Smith	The Welding Institute	U.K.
R.M.E.J.Spiering	Twente Technical University	The Netherlands
E.Vitale	Università di Pisa	Italy

PROBLEM DEFINITION AND DATA PROCESSING

Specifications

The specifications reproduced the geometry (see Fig.1) of one of the CT-specimens tested in the experimental round robin of the EGF working party on the measurement of crack extension. Material tensile properties measured from specimens taken from the vicinity of the CT-specimen were given in the form of a table reproduced here as Table 2. Furthermore, a large scale plot on millimetric paper represented the y-direction uniaxial tensile curve shown in small scale in Fig.2. Poisson's ratio was given as 0.3.

Participants were asked to report the load-displacement behaviour, J and COD up to a load point displacement V = 2 mm, supposing there was no crack growth. V was defined as the variation of the distance between points A and A' on the load line on opposite sides of the machined slot and initially 20 mm apart. The analyst could choose freely the way to introduce the material tensile properties and perform the analysis in plane strain, plane stress or 3D, whatever he considered to be the most representative.

TABLE 2 - Material Tensile Properties

	X	Y	Z	
0.2-yield stress	552	554	558	MPa
1	579	580	583	MPa
2	615	613	618	MPa
5	667	668	668	MPa
UTS	672	676	670	MPa
Uniform elongation	8	7.5	6	%
Total elongation	15.5	15.5	9.5	%

If a participant reported more than one solution, he was requested to declare which one he considered to be his best solution. Of course, all the options of the numerical analysis (mesh, loading steps, convergence tolerances, etc.) were to be chosen freely by each participant.

Data Processing

A glance at Figs.3-12 shows that they have a regular shape. Therefore the data tables delivered by the participants were reduced to raw data tables containing typically 10 to 20 points per curve. A curvilinear interpolation procedure was then applied in which 5-10 intermediate points between the raw data points were calculated. The resulting curves pass exactly through the raw data points and appear as having a continuous slope. Care was taken not to miss the waviness or the humps appearing in some solutions. The participants were requested to check the raw data tables and the plots produced from them.

Types of Solution

A total of 43 different solutions were submitted by the participants. They can be classified as follows:

19 basic plane strain solutions
8 basic plane stress solutions
4 3D solutions
12 complementary solutions using different options from the participant's basic solution, e.g. a different stress-strain curve.

The latter category is not discussed hereafter. However, some conclusions that these solutions allow to draw on the influence of various parameters will be noted en passant.

CODES AND DISCRETIZATION

Finite Element Codes

All participants used finite element codes which are listed in Table 3 together with some indications on the numerical procedure adopted. Except ADINA (6 participants), MARC (two participants) and NONSAP (one participant) the other codes are here termed as own. The incremental theory of plasticity and the von Mises yield criterion with the associated flow rule were applied in all codes. Hardening was treated as isotropic except by participant 9 who used the basically kinematic fraction model.

To give an account on the iteration procedure adopted in each code would require too much space without being complete because many participants did not document these aspects sufficiently. Iterations within each

TABLE 3 - Finite Element Codes and Numerical Methods

Participant	Code	Numerical method	Iteration for each step	Number of loading steps	V_{max} (mm)
1	ADINA 78	Tangent modulus	yes	50	2.1
2	ADINA	Tangent modulus	yes	10	2.9
3	Own	Initial strain	yes	10	2.2
4	Own	Initial stress	yes	11	2.1
5	ADINA 77	Tangent modulus	yes	10	2
6	MARC J-2	Tangent modulus	yes	19	2.2
7	Own	Initial stress	yes	150	2.2
8	Own	Initial stress	yes	17	1.2
9	Own	Modified tang mod.	yes	26	1.9
10	NONSAP	Tangent modulus	yes	63	2
11	Own	50% initial stress 50% tang mod.	yes	29	2
12	Own	Tangent modulus	yes	36	2
13	Own	Tangent modulus	no	85	2
14	ADINA 78	Tangent modulus	yes	16	2.3
15	MARC J-2	Tangent modulus	yes	9	2
16	Own	Tangent modulus	yes	114	2
17	ADINA	Tangent modulus	yes	20	3.7
18	Own	Initial stress	yes	39	1.6
19	Own	Tangent modulus	yes	28	2.4
20	Own	Initial stress	yes	110	2.3
21	ADINA 81	Tangent modulus	yes	60	2.1
22	Own	Tangent modulus	no	32	1.9

loading step were performed in most codes until some convergence criterion was reached. This criterion used some norm of the iterative changes in the force unbalance vector or in the displacement vector, or was based on energy balance or on the satisfaction of the plasticity rule. Table 3 shows the number of loading steps chosen by each participant for his "best solution" up to the maximum displacement value indicated in the last column.

Discretization

Table 4 is a condensed presentation of the discretizations used in the 2D solutions. It can be seen that 8-node isoparametric quadrilaterals alone or in combination with 6-node triangles were by far the favoured type of element since they were applied by 14 participants. One used 12-node quadrilaterals, five 4-node quadrilaterals alone or combined with 3-node triangles and one participant only 3-node triangles. The ratio of the maximum number of degrees of freedom (984, participant 18) and the minimum one (251, participant 5) was almost 4. All participants modelled one half of the specimen due to symmetry. 3D solutions will be discussed separately in a later section.

Representation of the Uniaxial Stress-Strain Curve

Figure 2 shows that for the given material a bilinear representation can approximate the material tensile curve quite closely up to a strain of about 2.5%. Indeed, three participants had adopted a bilinear law in all or some of their solutions. Three participants adopted a power law and the others a multilinear representation. Between 0.4% and 2% strain even the crudest approximations were within 3% of the experimental curve.

TABLE 4 - Finite Element Models - 2D Solutions

Participant	DOF	Elements	Far field elements (a) Q12	Q8	T6	Q4	T3	Crack tip elements Singularity	Size (mm)
1	464	67		x				1/r	0.1
2	970	184		x	x			no	2
3	324	176				x	x	no	1.25
4	380	51		x				1/r	1.3
5	251	34		x				1/r	3.4
6	367	53		x				1/r	0.6
7	637	94		x				no	0.5
8	440	32	x					1/r	5
9	360	310					x	no	0.5
10	474	76		x	x			no	1.32
11	581	81		x				$1/\sqrt{r}$	0.315
12	319	46		x				no	1
13	403	166				x		1/r	0.5
14	985	143		x				1/r	1
15	310	44		x				1/r	1.25
16	592	275				x	x	no	0.2
17	431	59		x				1/r	2.02
18	984	150		x	x			no	0.75
19		309				x	x	no	0.635
20	551	246				x		no	0.5
21(b)									
22	564	84		x				no	0.59

(a) Q12, Q8 and Q4: 12-node, 8-node and 4-node isoparametric quadrilaterals, respectively. T6 and T3: 6-node and 3-node triangles.
(b) Gave only a 3D solution.

It seems therefore that the way in which the uniaxial stress-strain curve was represented is unimportant as to its effects on the scatter of the results.

COMPARISON AND DISCUSSION OF THE SOLUTIONS

Best Solutions

Figure 3 shows the load versus displacement response and Fig.4 J versus load of the participants' best solutions. There are 21 curves, because participant 2 did not declare which one of his two solutions, plane stress and plane strain, he considered to be the best one.

The wide scatter of the results is striking. Experimental results are shown on these and the following figures. They were measured on the CT-specimen taken as the reference for the specifications, de Vries (3). In the test stable crack growth started at V = 0.9 mm which means that the comparison of the numerical results with the experiment is possible only up to that deformation. The last indicated experimental point at V = 1 mm includes already some stable crack growth. The experimental points on the J-plots represent values determined according to ASTM E813.

The four best solutions 5, 6, 12 and 21 close to the experimental results are 3D-solutions. Plane strain solutions are above and plane stress solutions below the experimental curve, referring to load values.

Figures 3 and 4 reflect the kind of scatter that can be expected from EPFM predictions. They are not very useful when one is interested in the reasons of this scatter. For this purpose it is better to look separately at the various types of solutions.

Plane Strain Solutions

P versus V, J versus P and COD versus P obtained from the plane strain solutions are shown on Figs.5, 6 and 7, respectively. It is of course interesting to look at the extreme results, particularly curves 3 and 8.

Participant 3 had previously applied the same code to EPFM problems with good success, however, using load control whereas in the present solution he applied imposed displacements. He discovered an error in the postprocessor calculating the nodal forces at imposed displacement nodes. Repeating the analysis with load control he obtained a load-displacement behaviour close to solution 2. He had never calculated COD before. Apparently the erroneous post-processor does not explain the anomalous behaviour of his J for which no convincing reason could be advanced.

Participant 8 applied 12-node quadrilaterals in a code that he declared to be still under development. The soft behaviour of his solution could not be explained up to the moment of writing this paper.

The other 17 plane strain solutions are within a much more reduced scatter band. Solution 17 shows an irregular behaviour above a load level of 70 kN, it predicted for V = 2 mm a load of 76 kN which is higher than for all other solutions except number 3. This seems to indicate some sort of instability of the integration process connected possibly with too loose convergence tolerances. The other few solutions on the stiff side, numbers 2, 9 and 19 show no systematic correlations between the positions of the curves and the features of the numerical analysis. Qualitatively, 3-node elements (no.9) and 4-node elements (no.19) are expected to give stiffer answers than more complex elements.

Solution 2 introduced a bilinear uniaxial stress-strain curve which was above the experimental one at all strains, this certainly introduced a few percent of overstiffness.

When judging the scatter of the results, it should be read vertically on Fig.5 and horizontally on Figs.6 and 7. In the latter cases, given a critical value of J or COD, the curves can be used for predicting the critical load.

Plane Stress Solutions

These are plotted in Figs.8, 9 and 10 for P versus V, J versus P and COD versus P, respectively. The waviness of the plane stress solution of participant 17 starts at a lower load than was the case in his plane strain solution, already below 1.5 mm displacement or 50 kN load.

As in the plane strain case, the scatter of J and COD prediction is comparable to that of the predicted load-displacement behaviour. There is no evident correlation between the grouping of the curves and the features of the numerical analysis.

3D Analysis

Table 5 shows the discretization adopted by the four participants who delivered a 3D solution. All four modelled one half of the thickness (of one

TABLE 5 - Finite Element Models - 3D Solutions

Participant	DOF	Elements	Type of elements	Crack tip elements Singularity	Crack tip elements Size (mm)
5	896	64	15 collapsed hexahedra (3 layers) with independent nodes at crack tip, surrounded by 30 isoparametric hexahedra with 20 nodes, and 19 isoparametric 8-node quadrilaterals in plane stress.	1/r	3.4
6	1129	53	6 collapsed hexahedra (1 layer) with independent nodes at crack tip, surrounded by 47 regular 20-node bricks (1 layer).	1/r	0.6
12	842	82	18 collapsed hexahedra (3 layers) surrounded by 36 regular 20-node bricks (3 layers) and 28 isoparametric 8-node quadrilaterals in plane strain.	no	1
21	867	66	24 collapsed bricks (3 layers) surrounded by 24 regular 20-node bricks (3 layers) and 17 isoparametric 8-node quadrilaterals in plane stress + 1 truss element.	1/r	3

half of the specimen). Participant 6 modelled the whole area by one layer of 3D elements whereas the others modelled the crack tip region by three layers of 3D elements and the remainder of the specimen in 2D, plane strain for No.12, plane stress for 5 and 21.

In spite of the large differences in discretization, the results shown in Figs.11 and 12 are within a very small scatter band and in agreement with the experimental results. The reported J values are through the thickness averages. It must be pointed out, however, that when plotting J versus V the curve of No.12 is about 30% below the other three predictions and the experimental curve. This participant in fact reported his J as unreliable due to an error in the numerical procedure.

These results indicate that 3D analysis can be performed in various ways, the important thing being that the crack tip region is modelled in 3D. If one is interested in global behaviour, not in the variation of J or COD across the thickness, it is sufficient to use one layer of brick elements on the half thickness.

Large Strain Analysis

A total number of seven different solutions were obtained from a large strain analysis. Four of these can be seen on Figs.3 and 4: numbers 1, 10 and 16 are plane strain solutions and 17 is a plane stress solution. In this round robin the strains remain small: at the maximum deformation the region where the equivalent strain exceeds 5% is small, less than about 10% of the ligament length in plane strain and 5% in plane stress. Therefore, results obtained from large strain analysis do not differ much from those of material non-linear only analysis.

The participants had nevertheless an interesting discussion on large strain analysis. Participant 1 has shown that only the updated Lagrangian (UL) formulation assures the incompressibility of plastic deformation. However, this conclusion was reached using ADINA in which indeed only the UL formulation seems to treat correctly the incompressibility of plastic deformation. Bathe and Ozdemir (4) have demonstrated that the UL and the total Lagrangian (TL) formulations can be written in such a way that identical numerical results are obtained, provided the correct material constitutive relations are introduced. In the TL formulation the uniaxial stress-strain curve should be given in terms of 2nd Piola-Kirchhoff stresses and Green-Lagrange strains whereas the UL formulation necessitates expressing this curve as Cauchy (true) stresses versus true (logarithmic) strain.

Determination of J

Most participants had calculated J from the path integral definition of Rice (5), generally taking the average of several paths. Five participants had used the virtual crack extension method alone or in addition to the path integral calculation. The reported deviations of the minimum and maximum value of the path integral from the average were always smaller than 6%.

When discussing path dependence one must distinguish between real path dependence and local variations depending on the discretization. Bakker (6) has shown that if J is calculated inside a ring of isoparametric 8-node finite elements, there is a large local variation between the three possible paths passing through the integration points of the 3x3 integration scheme. In a typical case

inner path: $J = 0.917 \times J_{mean}$

central path: $J = 1.16 \times J_{mean}$

outer path: $J = 0.84 \times J_{mean}$

where J_{mean} is the average of the 3 paths. However, Bakker has demonstrated that J_{mean} is theoretically and numerically equal to the value of J obtained by the virtual crack extension method. If J is determined by the path integral calculation, it is therefore recommended to use the averaging procedure inside different rings of finite elements for studying the path dependence of J. Other kinds of averaging procedures than that described above are possible. By passing the integration paths through the Gauss integration points instead of through the nodes, the following advantages are obtained:

a) at the integration points the required derivatives are available;
b) one takes advantage of the Gauss integration scheme avoiding the accumulation of integration errors along the integration path.

If a 2x2 integration scheme is used, the average of the two paths can be taken inside each finite element ring.

The participants agreed that the determination of J by the virtual crack extension method is considered to offer many practical advantages over the path integral calculation. Two formulations of the virtual crack extension method are available, i.e. that by Parks (7) and by de Lorenzi (8). The latter has the advantage that the results are independent of the size of the virtual crack extension, as the required partial derivatives with respect to the crack length are determined analytically. The formulation of ref.(7) determines these partial derivatives by numerical differentiation, which makes the results dependent on the size of the virtual crack extension, which hence should be chosen with care.

Determination of COD

The specified linear extrapolation to the crack tip position worked well. However, this conclusion was reached for the case of deep edge cracks, when the crack flanks show an extended linear portion. It is recommended to perform a linear extrapolation of the straight region of the crack flanks to the crack tip position by using some numerical procedure. Hand-made extrapolation is not only unnecessarily elaborate but also leads to a wavy COD versus V or P curve. The numerical procedure could be simply the "experimental" method: one node in the region of the crack mouth and the second node on the crack flank not too close to the crack tip in order to be sure that it is still on the straight portion of the crack flank. Also, a linear best fit to several nodes can be performed. In all cases it is recommended to check the validity of the choice of the points used for the extrapolation, by plotting the crack profile or by calculating numerically the deviations of various crack flank nodes from the adopted straight line.

In the vicinity of the crack tip the deformed crack shape depends on the mesh and the type of singularity, if any. This will be discussed below.

Type of Singularity

Although one half of the participants did not use singular crack tip elements, such elements appeared however to be the favoured procedure. Some of those who had not used singular crack tip elements declared that they would prefer to make use of them in the case they would have larger size elements. The advantage of singular crack tip elements was considered to be that even with a coarse mesh the crack flank shape is realistic (corresponding to measurement) whereas regular elements give a too stiff behaviour, whatever the mesh refinement. Especially in 3D problems (surface cracks) it seems important to obtain a more realistic prediction of local behaviour along the crack front. Further justifications advanced in favour of singular crack tip elements were:

- they give small differences between J values from the three integration paths passing through the integration points of the first ring of (collapsed) finite elements whereas regular elements give large differences;
- in small strain analysis the strain energy density shows theoretically a 1/r singularity which, since stresses are bounded, gives the same singularity for strains.

However, the following points of view were expressed in favour of using non-singular elements:
Non-singular collapsed elements increase the number of incompressibility constraints. For instance, for the usual 8-node element with straight sides, the ratio DOF/constraints is 1 and if this element is collapsed the ratio becomes 2/3. The more of these collapsed elements are used to model the crack tip region, the more constraints are introduced, resulting in a too high stiffness. Lamain (9) has shown that by modifying the shape functions, however, the ratio DOF/constraints can be made again 1. This non-singular modified collapsed element might be able to compete favourably with the singular collapsed element, as it does not have the more or less disturbing unbounded terms in the stiffness matrix.

Extrapolation to Larger Deformations

There is an interesting possibility to reduce computer time by stopping the analysis at some point well inside the elastic-plastic regime and extrapolating from there to the maximum deformation of interest. Such a procedure

was applied with success by participant 18 whose last data point was at V = 1.62 mm and who extrapolated up to V = 2 mm.

The extrapolation is valid as long as the assumption $\Delta a = 0$ holds in the extrapolated region and provided the last data point allows a correct definition of the regime beyond that point. In the present problem this condition can easily be checked, e.g. on the J versus V plot which is a straight line beyond V = 1 mm. In general cases it is more difficult to check where the analysis can be stopped. A possible procedure consists in plotting log J versus log (some displacement parameter), or versus log P (a loading parameter). The plot shows a straight line in the elastic regime followed by a bend and a second straight line corresponding to the elastic-plastic regime. The last data point must be well beyond the bend allowing to determine the second slope.

CONCLUSIONS

This round robin was defined in such a way as to represent the conditions in which the EPFM analyst has to work when solving a practical problem. The results showed a wide scatter between the "best solutions" of the participants meaning that EPFM numerical analysis is a delicate task.

Plane strain solutions were too stiff and plane stress solutions too soft, comparing with the experimental truth. Four 3D-solutions predicted correctly the experimental behaviour. Before 3D analysis is going to find a wider use, it is advisable to obtain more reliable answers from 2D analysis. Although e.g. the softest plane strain solutions were close to the experimental results, they must be considered as bad, since they are at the extreme side of the scatter band, the centre of which can be considered to be close to the "correct" plane strain result.

The reasons for the scatter could be only partly explained. The EGF working party on numerical analysis is going to perform a new round robin in order to develop better rules on how to do EPFM numerical analysis. This time the mesh and the stress-strain curve will be exactly the same for all participants. Since the purpose is to make code-to-code comparisons, it is not necessary to simulate the specimen. Therefore, the mesh will be simplified (holes and steps of the machined slot neglected) and a simple bi-axial stress-strain law will be adopted.

SYMBOLS

COD : crack tip opening displacement
J : path independent integral (5) experimentally determined according to ASTM E813
P : load, Fig.1
V : load point displacement, in Fig.1 the increase of the distance between A and A'

REFERENCES

1. Larsson,L.H., Int.J.Pres.Ves. & Piping, 11 (1983) 207.
2. Larsson,L.H., 3rd Int.Conf.on Num.Methods in Fracture Mechanics, Swansea, March 26-30, 1984.
3. de Vries,M., Personal communication,to be issued as an external ECN report in 1984.
4. Bathe,K.-J. and Ozdemir,H., Comp.& Str., 6 (1976) 81.

5. Rice,J.R., J.of Appl.Mech., 35 (1968) 379.
6. Bakker,Ad., Int.J.Pres.Ves. & Piping, 14 (1983) 153.
7. Parks,D.M., 1st Int.Conf.on Num.Methods in Fracture Mechanics, Paper 3.3, Swansea, UK (1978).
8. de Lorenzi,H.G., Int.J.of Fracture, 19 (1982) 183.
9. Lamain,L., 6th Int.Conf.on SMIRT, Paper M1/6, Paris, 1981.

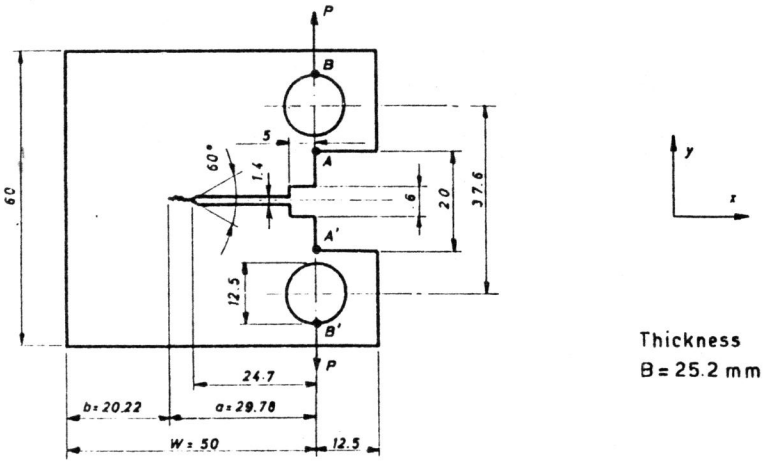

Fig. 1 - Geometry of the specimen

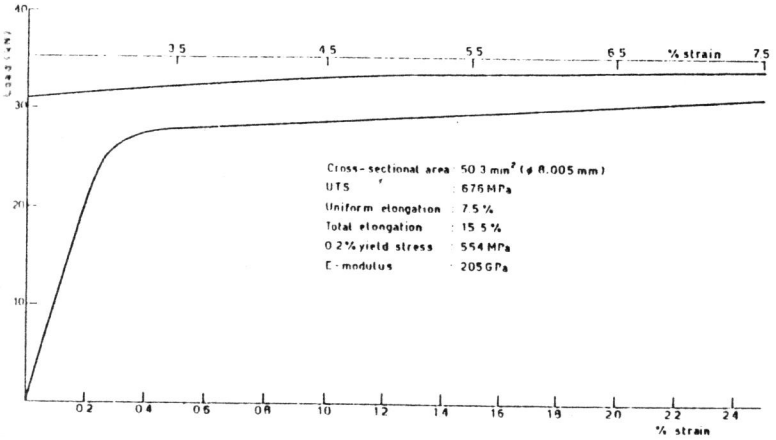

Fig. 2 - Uniaxial stress-strain curve

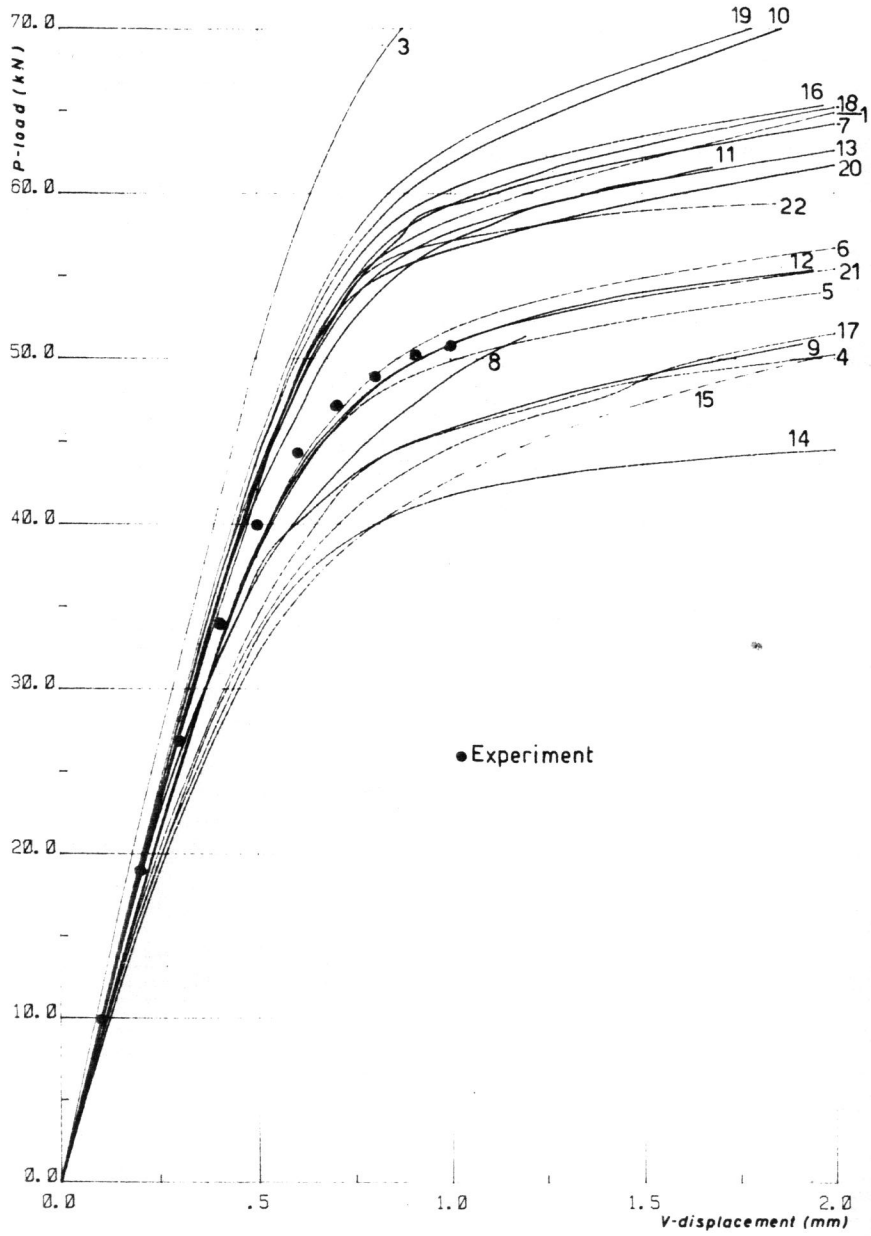

Fig. 3 - Best solutions, load versus displacement

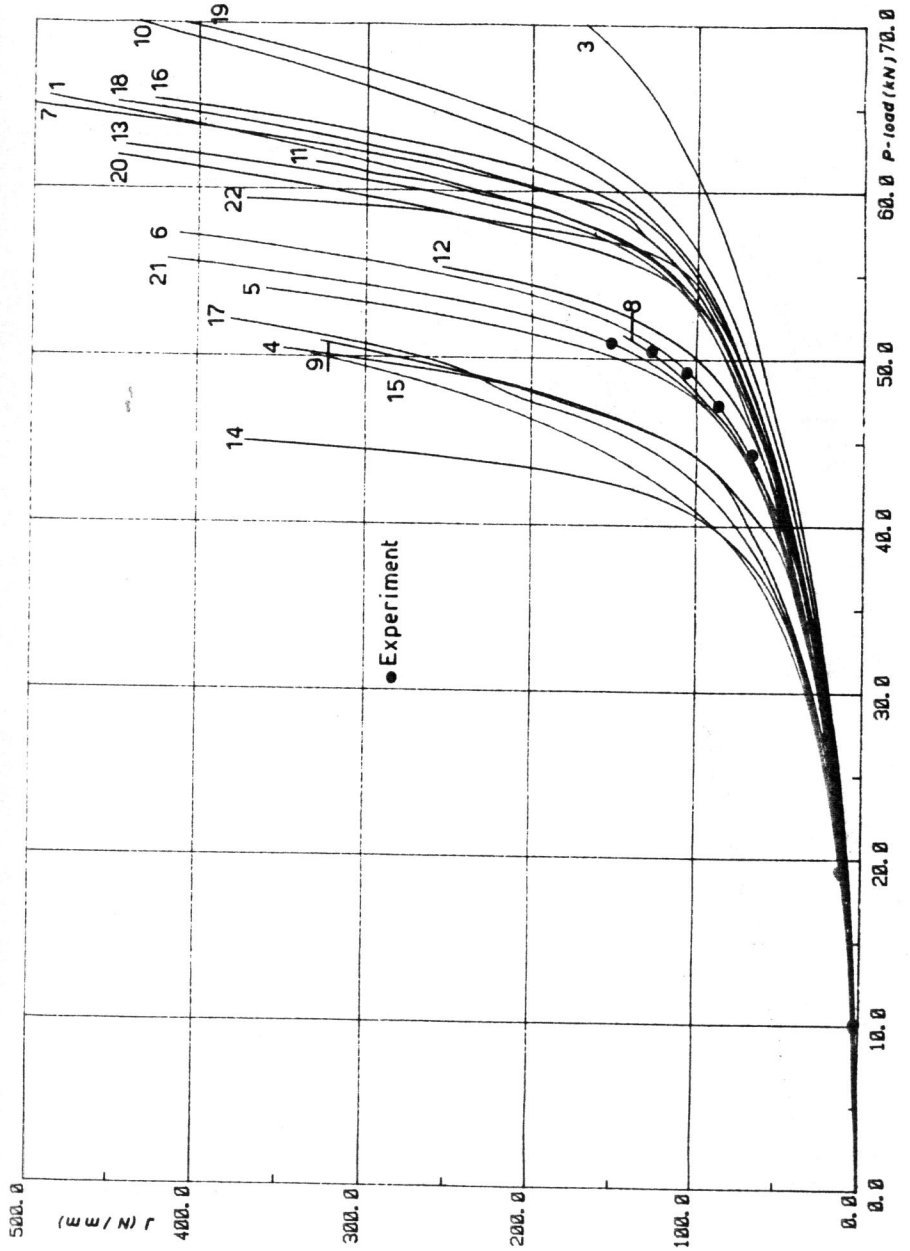

Fig. 4 - Best solutions, J versus load

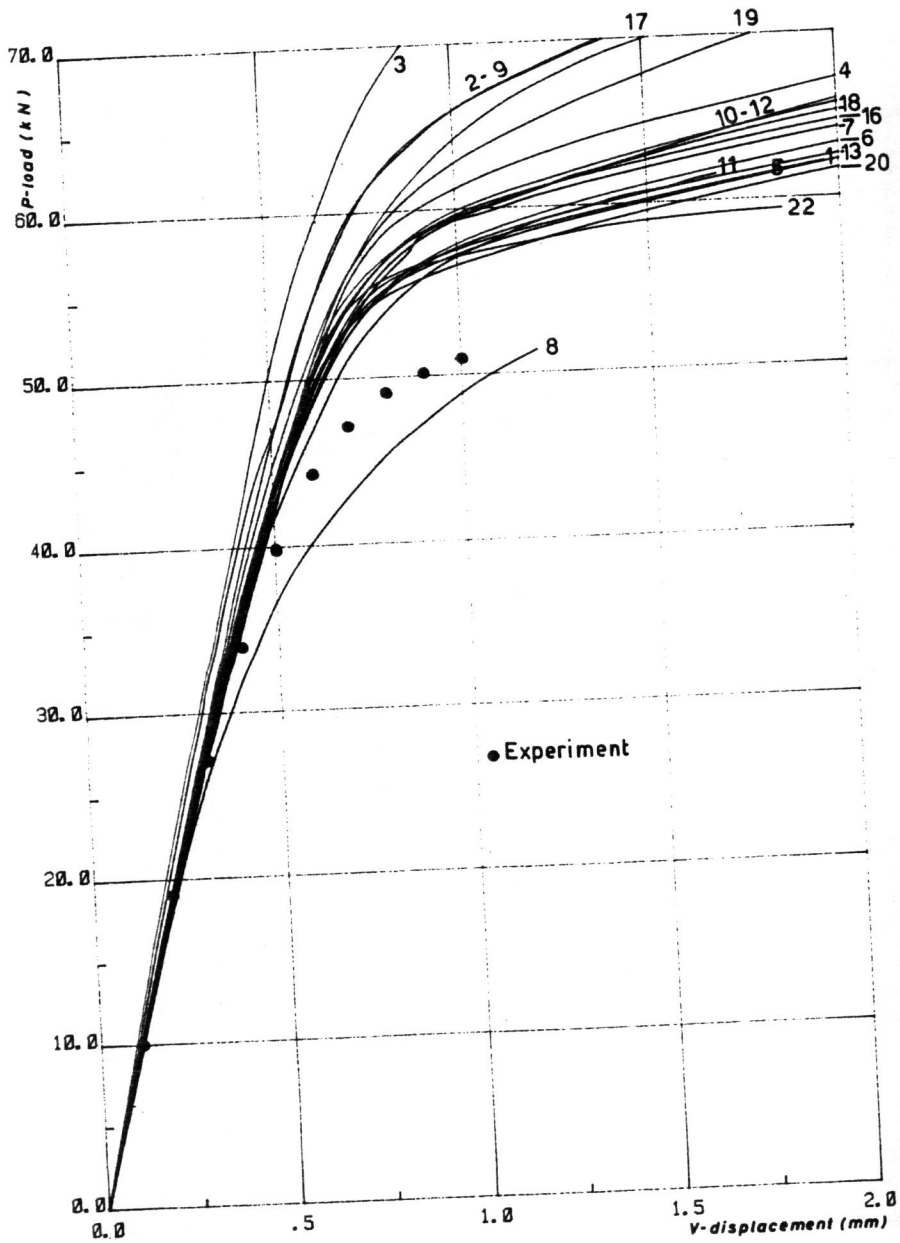

Fig. 5 - Plane strain solutions, load versus displacement

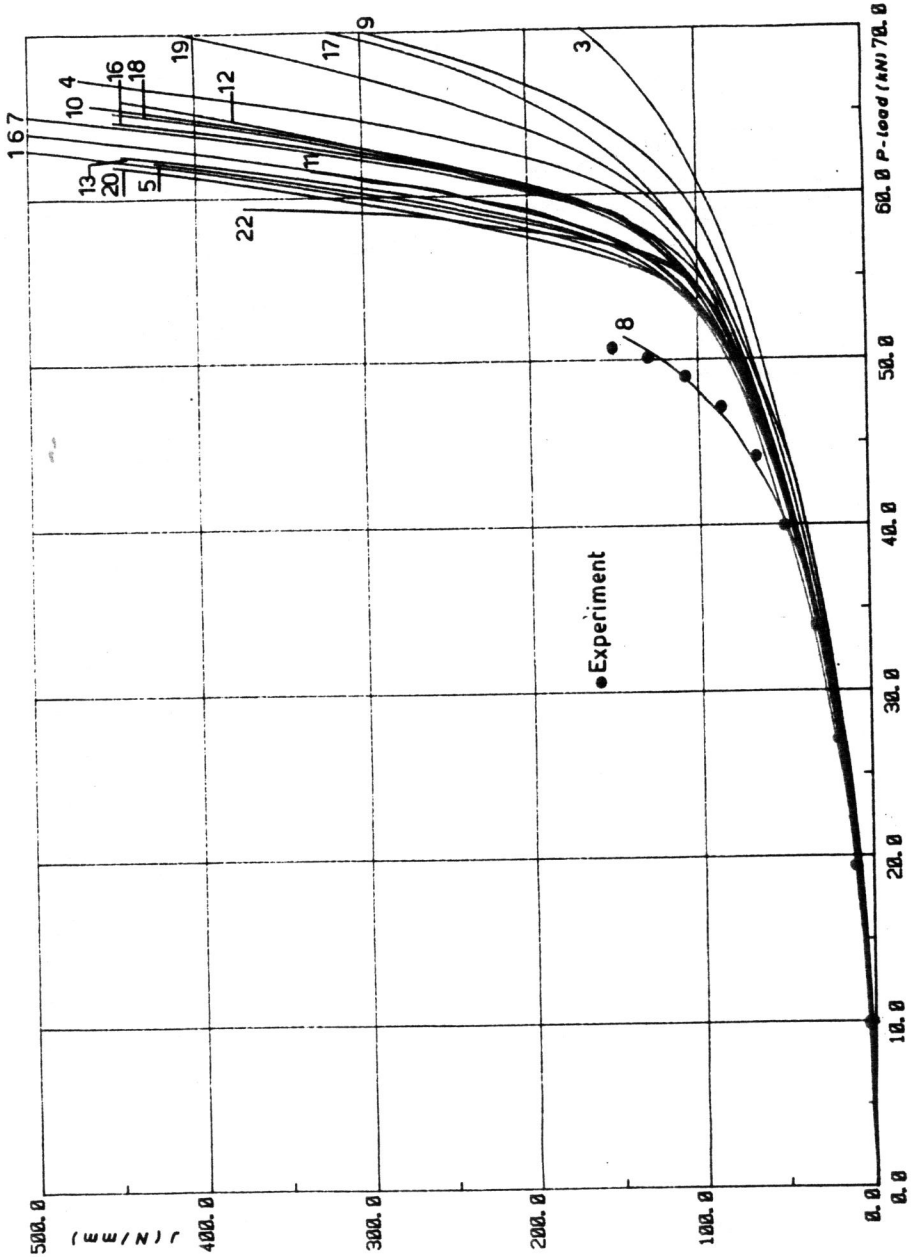

Fig. 6 - Plane strain solutions, J versus load

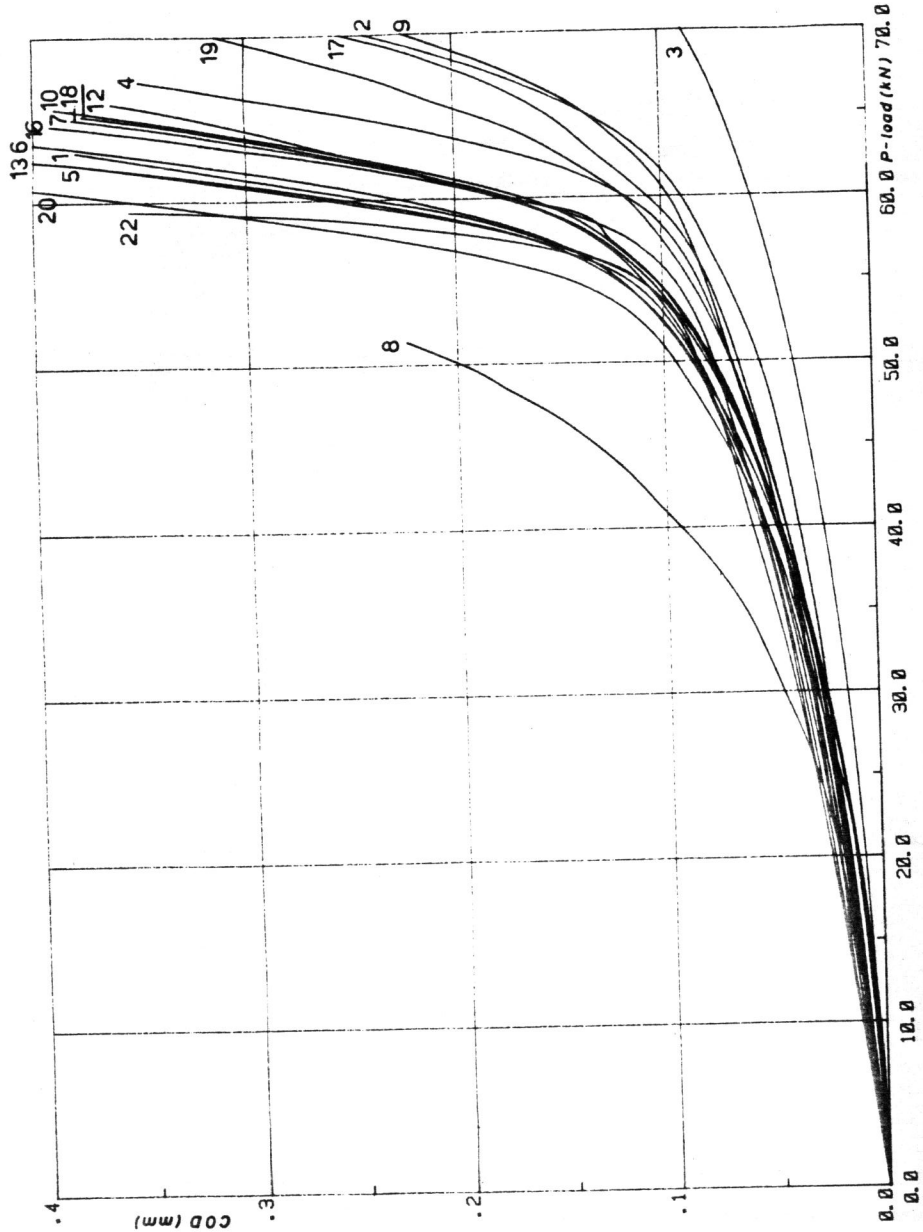

Fig. 7 - Plane strain solutions, COD versus load

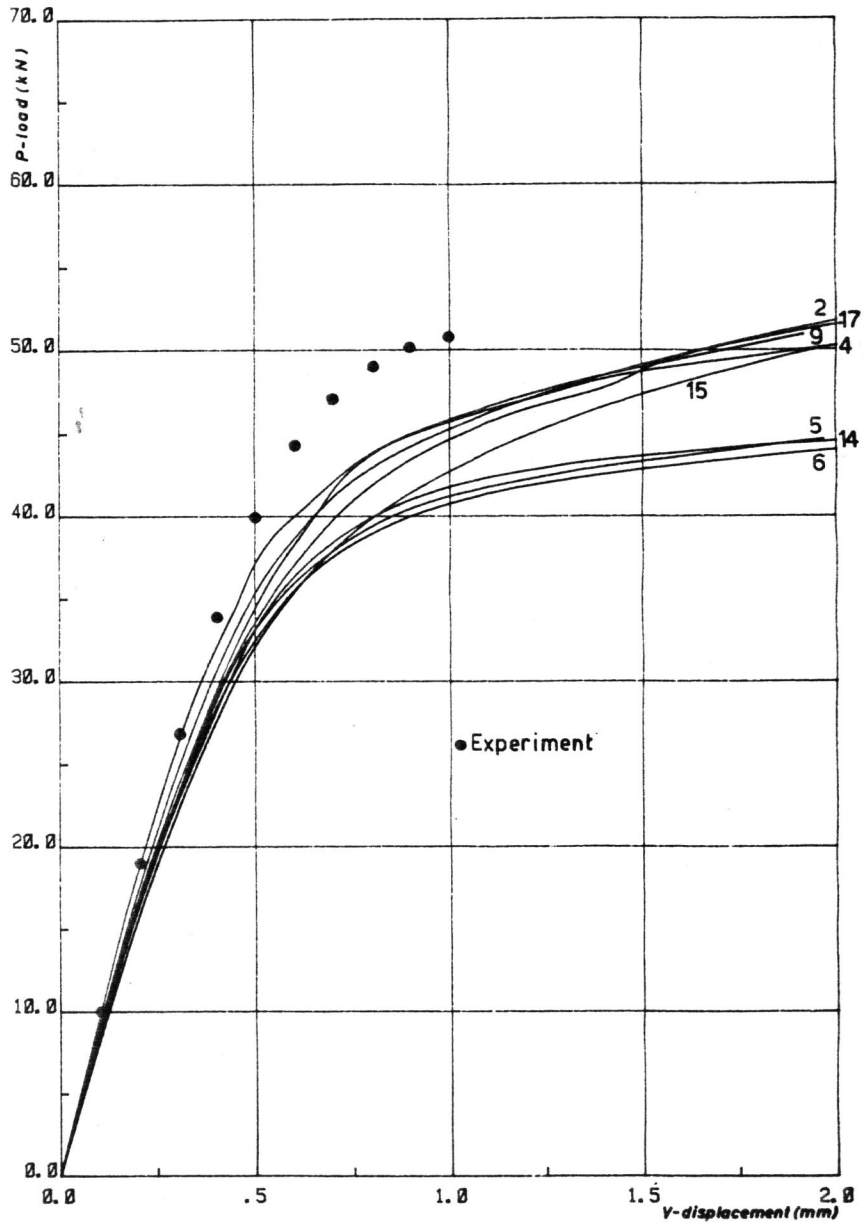

Fig. 8 - Plane stress solutions, load versus displacement

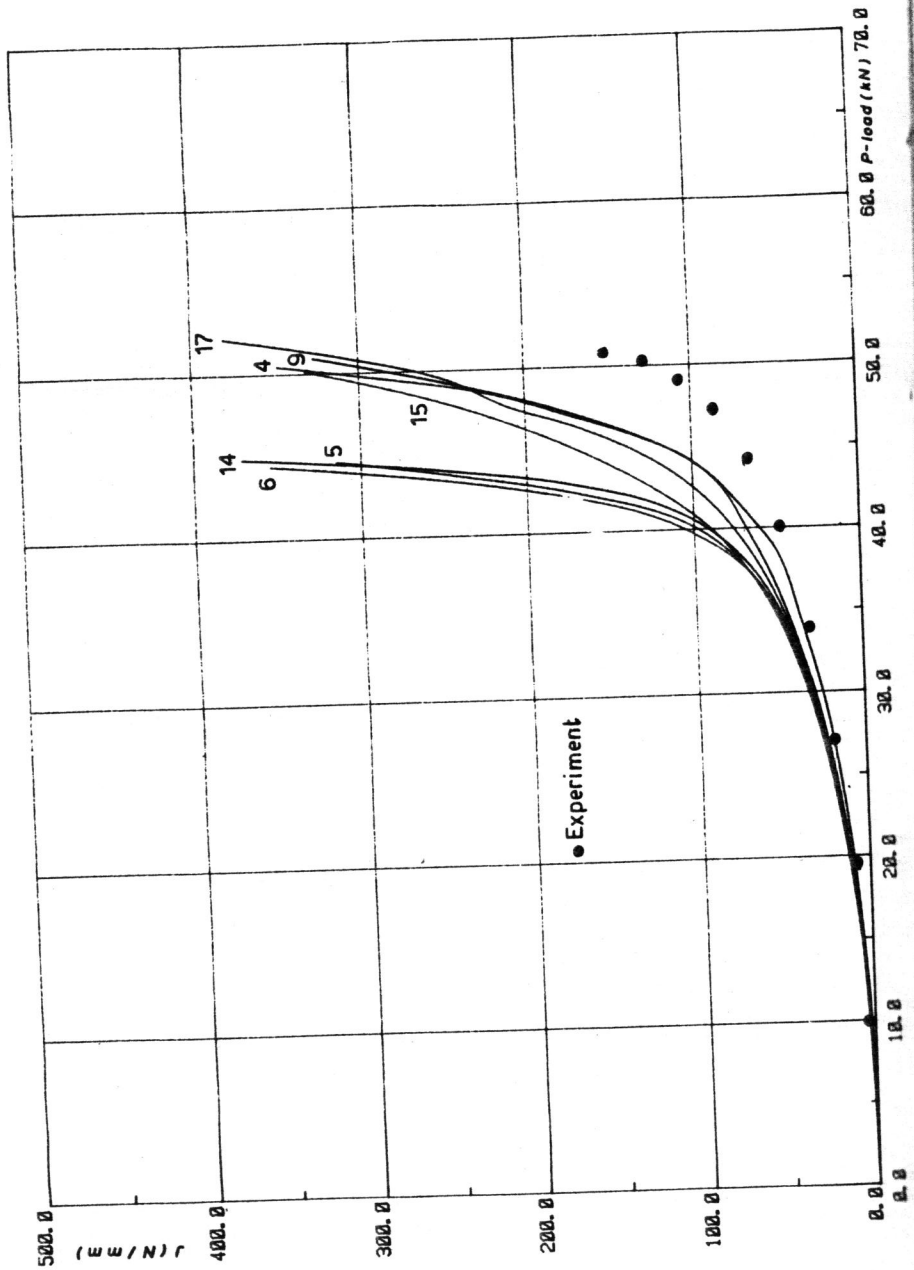

Fig. 9 - Plane stress solutions, J versus load

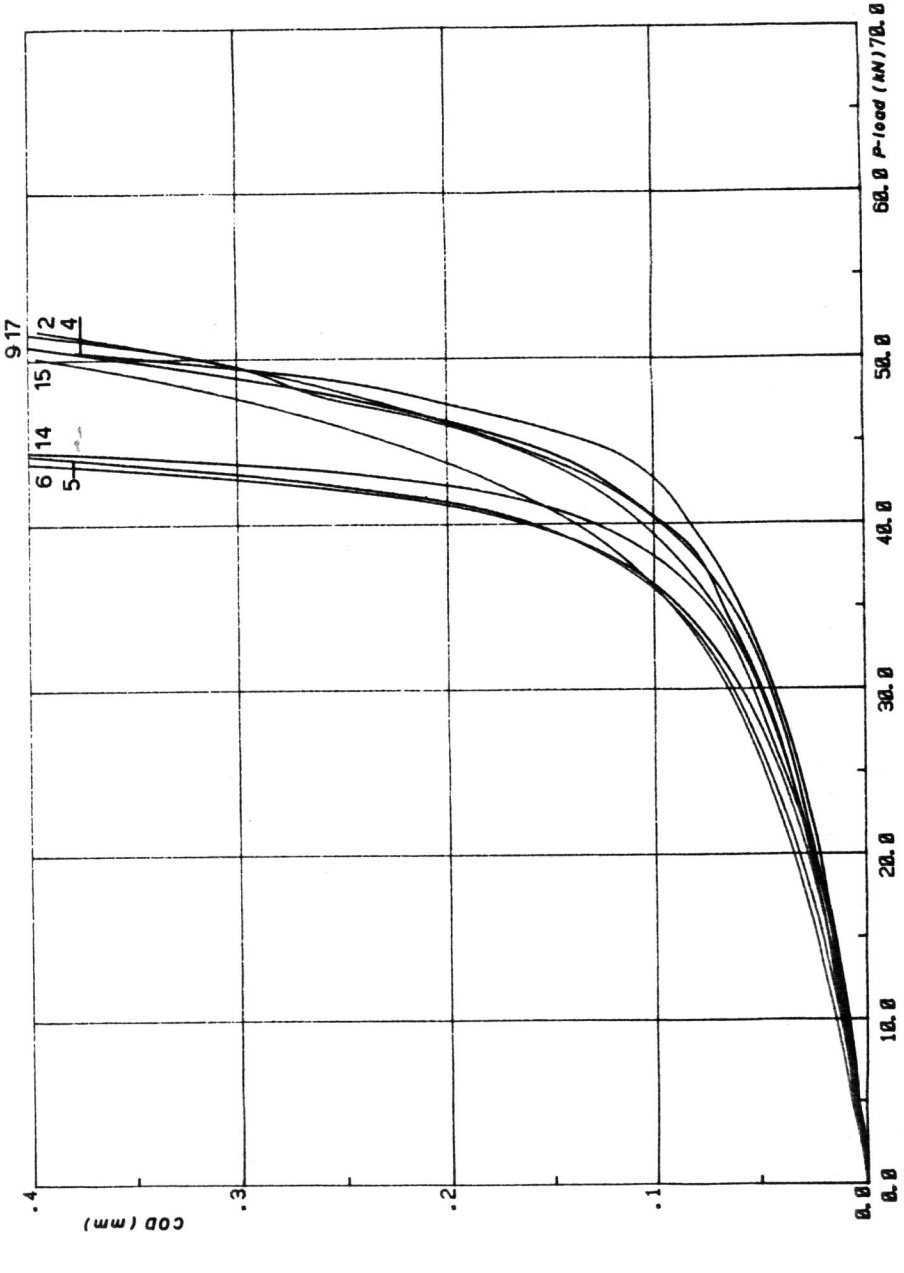

Fig. 10 - Plane stress solutions, COD versus laod

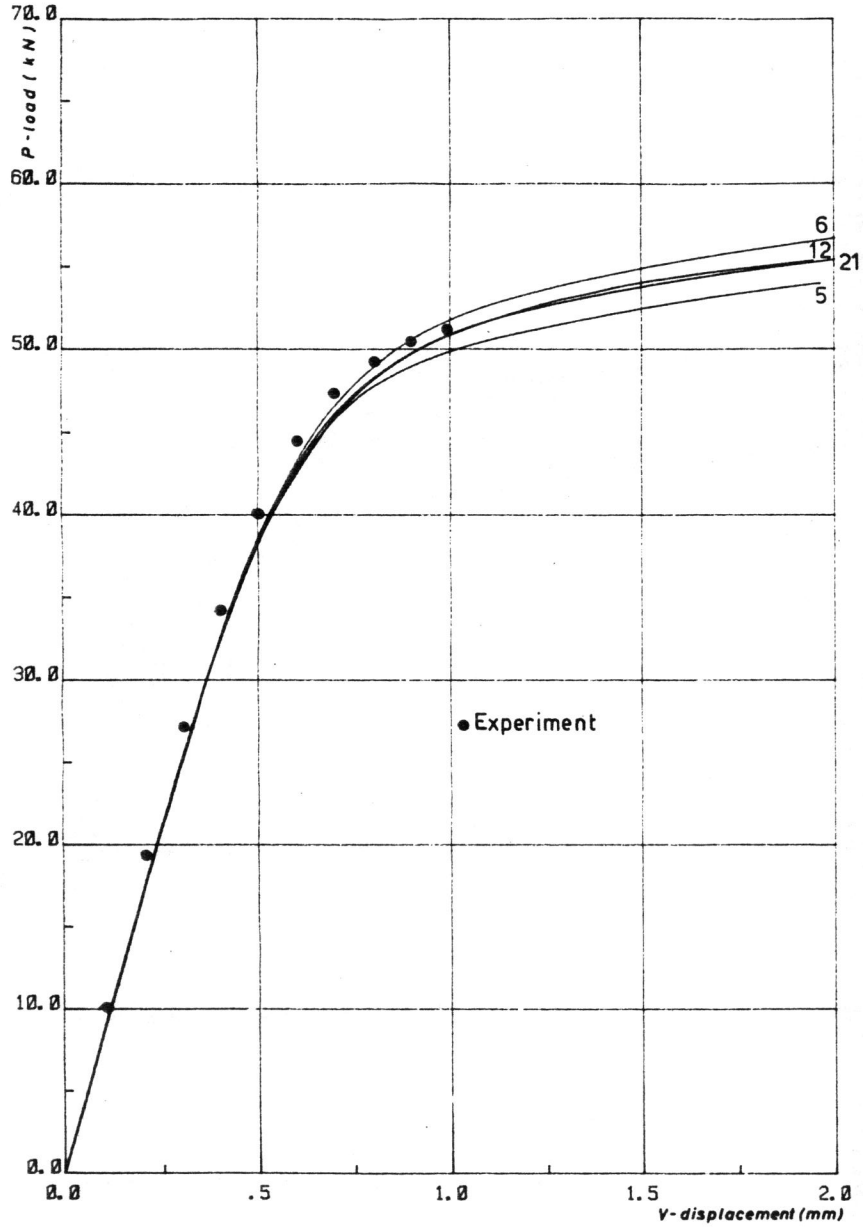

Fig. 11 - 3D solutions, load versus displacement

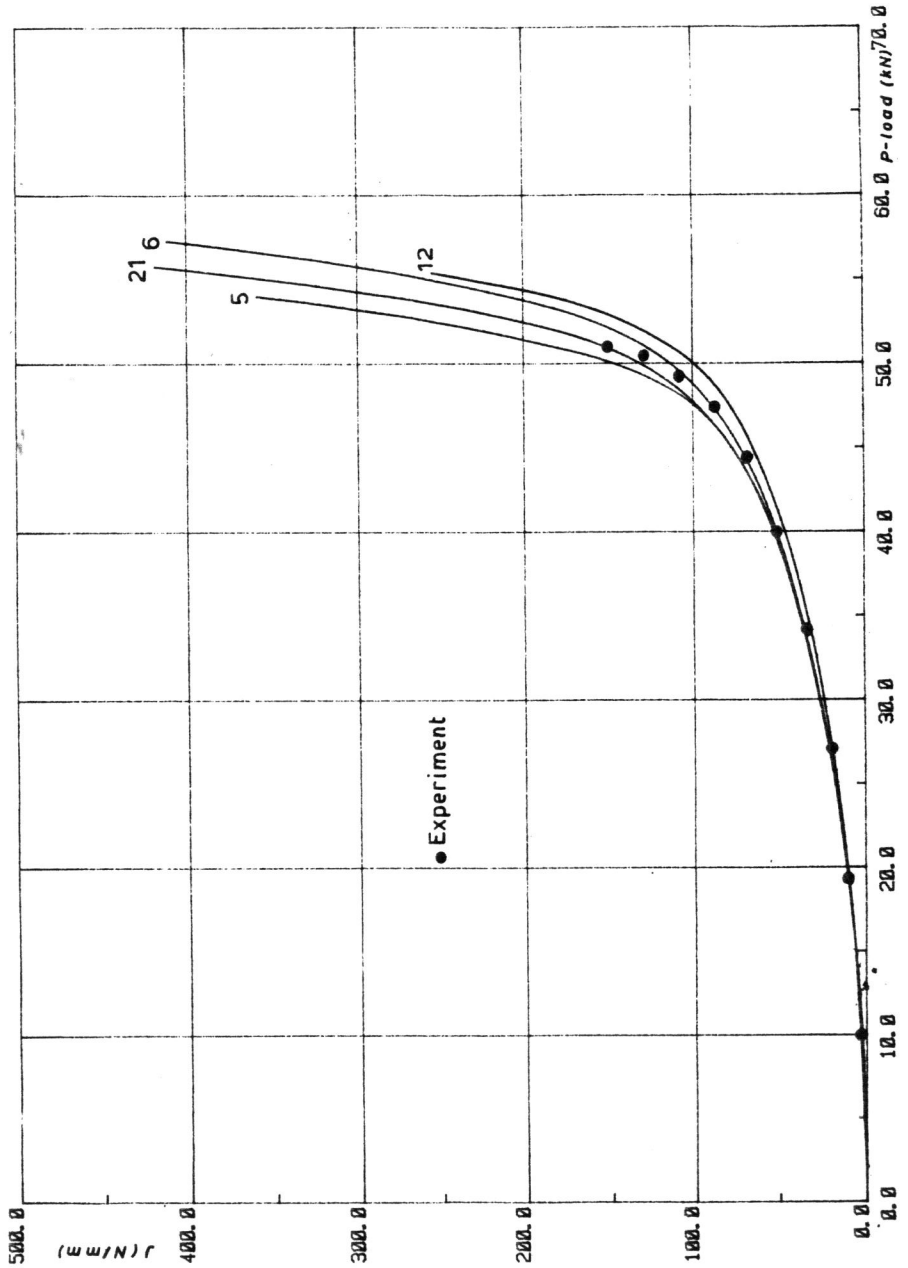

Fig. 12 - 3D solutions, J versus load